Molecular Crystals and Liquid Crystals Science and Technology. Section A. Molecular Crystals and Liquid Crystals

Publication details, including instructions for authors and subscription information:
http://www.tandfonline.com/loi/gmcl19

Biaxial Nematic Order in the Hard-boomerang Fluid

P. I. C. Teixeira [a], A. J. Masters [b] & B. M. Mulder [c]

[a] Cavendish Laboratory, Madingley Road, Cambridge, CB3 0HE, United Kingdom

[b] Department of Chemistry, University of Manchester, Oxford Road, Manchester, M13 9PL, United Kingdom

[c] FOM Institute for Atomic and Molecular Physics, Kruislaan 407, NL-1098 SJ, Amsterdam, The Netherlands

Version of record first published: 04 Oct 2006

To cite this article: P. I. C. Teixeira, A. J. Masters & B. M. Mulder (1998): Biaxial Nematic Order in the Hard-boomerang Fluid, Molecular Crystals and Liquid Crystals Science and Technology. Section A. Molecular Crystals and Liquid Crystals, 323:1, 167-189

To link to this article: http://dx.doi.org/10.1080/10587259808048440

Mol. Cryst. Liq. Cryst., Vol. 323, pp. 167–189
Reprints available directly from the publisher
Photocopying permitted by license only

Biaxial Nematic Order in the Hard-boomerang Fluid

P. I. C. TEIXEIRA[a,*], A. J. MASTERS[b] and B. M. MULDER[c]

[a] *Cavendish Laboratory, Madingley Road, Cambridge CB3 0HE, United Kingdom;*
[b] *Department of Chemistry, University of Manchester, Oxford Road, Manchester M13 9PL, United Kingdom;*
[c] *FOM Institute for Atomic and Molecular Physics, Kruislaan 407, NL-1098 SJ Amsterdam, The Netherlands*

(Received 12 May 1997; In final form 1 July 1997)

We consider a fluid of hard boomerangs, each composed of two hard spherocylinders joined at their ends at an angle Ψ. The resulting particle is nonconvex and biaxial. The occurence of nematic order in such a system has been investigated using Straley's theory, which is a simplificaton of Onsager's second-virial treatment of long hard rods, and by bifurcation analysis. The excluded volume of two hard boomerangs has been approximated by the sum of excluded volumes of pairs of constituent spherocylinders, and the angle-dependent second-virial coefficient has been replaced by a low-order interpolating function. At the so-called Landau point, $\Psi_{\text{Landau}} \approx 107.4°$, the fluid undergoes a continuous transition from the isotropic to a biaxial nematic (B) phase. For $\Psi \neq \Psi_{\text{Landau}}$ ordering is *via* a first-order transition into a rod-like uniaxial nematic phase (N_+) if $\Psi > \Psi_{\text{Landau}}$, or a plate-like uniaxial nematic (N_-) phase if $\Psi < \Psi_{\text{Landau}}$. The B phase is separated from the N_+ and N_- phases by two lines of continuous transitions meeting at the Landau point. This topology of the phase diagram is in agreement with previous studies of spheroplatelets and biaxial ellipsoids. We have checked the accuracy of our theory by performing numerical calculations of the angle-dependent second virial coefficient, which yields $\Psi_{\text{Landau}} \approx 110°$ for very long rods, and $\Psi_{\text{Landau}} \approx 90°$ for short rods. In the latter case, the I–N transitions occur at unphysically high packing fractions, reflecting the inappropriateness of the second-virial approximation in this limit.

Keywords: Biaxial nematic phase; molecular theory; Onsager approximation

PACS Numbers: 64.70. M, 64.60. C

* Corresponding author. Tel.: +44 1223 337357; Fax: +44 1223 337000; e-mail: pt214@cus.cam.al.uk

I. INTRODUCTION

The search for biaxial nematic phases has been going on for over a quarter century, and is as alive as ever. Indeed it was realised early on that the molecules of most nematogenic compounds do not possess rotational invariance about their long axes, thus opening up the possibility of simultaneous macroscopic ordering along a second direction, perpendicular to the usual nematic director.

The first theoretical prediction of a biaxial nematic is due to Freiser [1], who generalised the Maier-Saupe model [2, 3] to include one biaxial order parameter. Shih and Alben reached the same conclusion on the basis of a lattice theory [4]. Later, Alben's Landau approach [5] established what seems to be the definitive topology of the phase diagram of biaxial objects: there exists a special critical point (the Landau point), corresponding to a given (biaxial) particle shape, at which the isotropic-to-nematic (I–N) transition is continuous and into a biaxial phase; this point separates two regimes where the transition is first-order into a rod-like (N_+) or a plate-like (N_-) uniaxial phase. Furthermore, uniaxial and biaxial phases are separated by two critical lines meeting the I–N boundary at the Landau point. (For a review of the Landau theory of the I–N transition see [6]).

However, it was not until the work of Straley [7] that the full set of order parameters required to describe a biaxial nematic phase, was appreciated. Straley's phase diagram of rectangular hard parallelepipeds is topologically identical to Alben's, as is that of Boccara, Mejdani and de Seze [8], who studied a fluid of asymmetric ellipsoids interacting *via* an infinite-range isotropic potential. One of us (BMM) has brought the machinery of bifurcation theory to bear on the problem [9], but his analysis of isotropic symmetry breaking in fluids of rectangular-slab-like particles (spheroplatelets and Straley parallelepipeds) was restricted to low densities owing to the Onsager second-virial approximation employed [10]. This was improved upon by Holyst and Poniewierski [11], whose smoothed-density approximation for the free energy [12] yielded *a priori* more reliable estimates for the transition densities (but the same location for the Landau point of spheroplatelets and biaxial ellipsoids, in terms of particle shape parameters, as Onsager theory) [13].

Their elegance and computational ease notwithstanding, the bifurcation analyses of Mulder, and of Hołyst and Poniewierski, tell us nothing about the nature of the uniaxial–biaxial transitions, nor can one use them to calculate the nematic order parameters (say, as functions of the density or temperature). By contrast, all these are accessible in the molecular theory of

Luckhurst and co-workers [14], which is similar to Straley's [7] in that the excluded volume interaction is mimicked by an interpolating 'potential'. A recent simulation [15] of a lattice system characterised by a similar potential [16] bore out only qualitative agreement with theory; again the phase diagram is compatible with the Alben topology. Tjipto-Margo and Evans' [17] Parsons-Lee [18, 19] treatment of the biaxial hard ellipsoid fluid, on the other hand, is restricted to the isotropic-uniaxial transition, but is otherwise in fair agreement with Allen's [20] and Camp and Allen's [21] simulation results. Finally, Sarman [22] has found a biaxial phase in a simulation of a variant of the Gay-Berne fluid.

Work has also been performed on rod-plate mixtures, where now the biaxiality is tuned by varying the composition [23–26]. Yet it appears that the biaxial nematic phase is often unstable with respect to de-mixing into rod-rich and plate-rich unaxial phases, both in Maier-Saupe [27–29] and hard-body [30–33] systems. Moreover, there are some indications [34, 35] that, under certain circumstances, the Landau point may split into two continuous transitions, I–(uniaxial)N and (uniaxial)N–B, an intriguing departure from the 'canonical' picture.

In the meantime, all was not quiet on the experimental front. The announcement of the first biaxial lyotropic liquid crystal (LC) [36] was followed by a spate of claims of observations of its thermotropic counterpart [37–42], which are not, however, beyond dispute [43].

We are interested in the nematic phases of LC dimers [44, 45]. These have been studied previously [46] in the context of the theory of Ref. [16]; here we shall model them as hard boomerangs (HBs). A HB consists of two hard spherocylinders, each of length L and diameter D, joined at their ends at an angle Ψ (see Fig. 1 below). On varying Ψ between 0° and 180°, such a particle goes from (uniaxial) rod-like to plate-like (for $\Psi \sim 90°$) and back to rod-like; it is non-convex, and biaxial for all Ψ other than 0°. Because we can draw on an extensive body of knowledge of the statistical mechanics of (mostly convex) hard bodies, this is a convenient model with which to investigate the effect of particle biaxiality on the phase diagram.

This Paper is organised as follows: in Section II we derive our theory and discuss the validity of several simplifying approximations, and how they may restrict its range of applicability. Then in Section III we present our results for the limits of stability of the nematic and isotropic phases of the HB fluid (from microscopic theory and bifurcation analysis, respectively), as well as for I–N coexistence (numerically from microscopic theory). We conclude in Section IV.

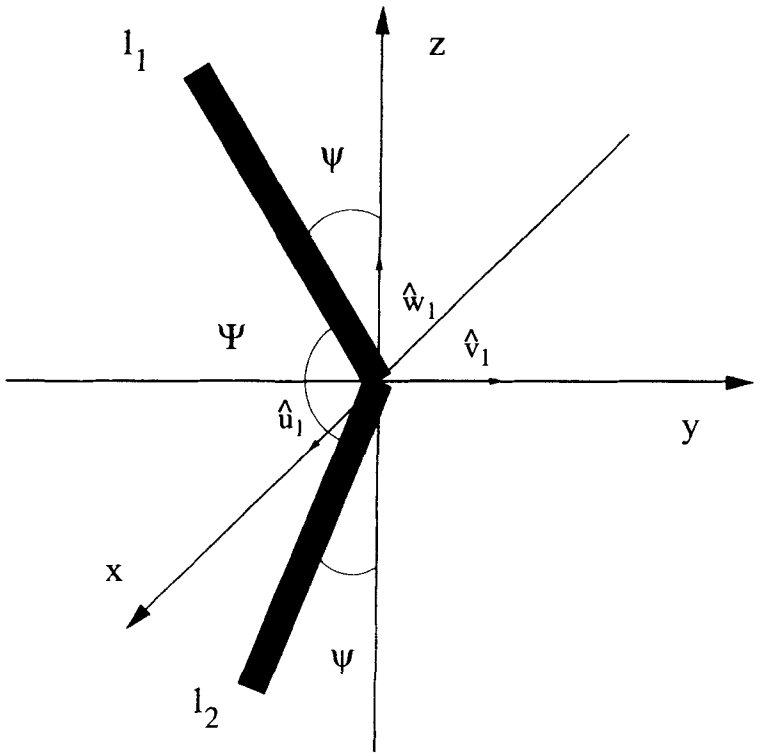

FIGURE 1 Hard boomerang in the xz-plane. The lab-fixed frame is $\{\hat{\mathbf{x}}, \hat{\mathbf{y}}, \hat{\mathbf{z}}\}$, and the particle-fixed frame is $\{\hat{\mathbf{u}}_1, \hat{\mathbf{v}}_1, \hat{\mathbf{w}}_1\}$; the two frames are coincident in this realisation, with the x-axis coming out of the plane of the page. i_j denotes the jth arm of boomerang i, of length L and diameter D. The boomerang angles are related by $\psi = (\pi - \Psi)/2$.

II. THEORY

A. Density-functional Approach

In Onsager's second-virial theory, the free energy density of a nematic phase can be written [10]

$$\frac{f_N[\rho, \hat{f}(\Omega)]}{k_B T} = \frac{f_{id}(\rho)}{k_B T} + \rho \int d\Omega \hat{f}(\Omega) \log[8\pi^2 \hat{f}(\Omega)] + B_2[\hat{f}(\Omega)]\rho^2, \qquad (1)$$

where ρ is the density, $f_{id}(\rho)$ is the ideal gas contribution, $\Omega = (\phi, \theta, \chi)$ is the set of Euler angles [47] defining the passive rotation that transforms the particle-fixed frame $\{\hat{\mathbf{u}}, \hat{\mathbf{v}}, \hat{\mathbf{w}}\}$ into the lab-fixed frame $\{\hat{\mathbf{x}}, \hat{\mathbf{y}}, \hat{\mathbf{z}}\}$, $\hat{f}(\Omega)$ is the

orientational distribution function (ODF), and $B_2[\hat{f}(\Omega)]$ is the second virial coefficient, defined as

$$B_2[\hat{f}(\Omega)] = -\frac{1}{2V}\int d1\, d2 \hat{f}(\Omega_1)\{\exp[-\phi(12)/(k_B T)] - 1\}\hat{f}(\Omega_2). \quad (2)$$

In Eq. (2), V is the volume of the system and $\phi(12)$ is the intermolecular potential, with $i = 1,2$ denoting the set of positional, as well as orientational, coordinates of particle i.

In the case of hard particles, the Mayer f-function $\Phi(12) = \exp[-\phi(12)/(k_B T)] - 1 = -1$ for overlapping geometries ($\phi(12) = \infty$) and $\Phi(12) = 0$ otherwise ($\phi(12) = 0$), hence $B_2[\hat{f}(\Omega)]$ reduces to the (ODF-weighted) integral over orientations of the (angle-dependent) excluded volume of two molecules:

$$B_2[\hat{f}(\Omega)] = \frac{1}{2}\int d\Omega_1\, d\Omega_2 \hat{f}(\Omega_1) v_{\text{excl}}(_{12}) f\,(_2). \quad (3)$$

This latter function is not known analytically for any non-convex particle shapes, and thus needs to be found numerically. Rather than undertaking this (rather heavy) computational task, we opted for, in this first approach, approximating the excluded volume of two HBs by the sum of excluded volumes of pairs of their constituent spherocylinders. This 'super position approximation' amounts to treating the spherocylinders as independent particles, and will introduce errors of (leading) order LD^2. However, these will be vanishingly small relative to the 'unperturbed' term (of order DL^2 [48]) in the limit of very long, thin spherocylinders, $D/L \to \infty$ [49], where Onsager theory is applicable. One additional limitation is that we do not recover the correct limit when $\psi = (\pi - \Psi)/2 \to \pi/2$. The quantitative reliability of the present strategy will be assessed in Subsection III.B.

In order to render the problem more easily tractable, we shall introduce one further simplification. Instead of working with the angle-dependent excluded volume in its general form, we shall follow Straley [7] and consider just the values it takes for a finite number of relative orientations of the two particles. Assuming particle 1 to be located at the origin of the lab frame, *i.e.*, $(\phi_1, \theta_1, \chi_1) = (\phi_0, \theta_0, \chi_0) = (0, 0, 0)$ (see Fig. 1), we compute the excluded volumes for the six distinct orientations particle 2 can have subject to the constraint that its long and short axes are directed along the coordinate axes [50]; these are listed in Table I (compare with Tab. I in [7]). In the spirit of Straley's treatment, we then fit the entries in Table I to a second-order

TABLE I Excluded volumes for the six relative orientations of two particles for which particle 1 has the orientation $(\hat{\mathbf{u}}_0, \hat{\mathbf{v}}_0, \hat{\mathbf{w}}_0) = (\hat{\mathbf{x}}, \hat{\mathbf{y}}, \hat{\mathbf{z}})$, and particle 2 has its principal axes $(\hat{\mathbf{u}}, \hat{\mathbf{u}}, \hat{\mathbf{w}})$ along the different (lab) coordinate axes (see the text, Fig. 1 and Ref. [7] for details)

x	y	z	*(Excluded volume)*$/2DL^2$	ϕ	θ	χ
$\hat{\mathbf{u}}$	–	$\hat{\mathbf{w}}$	$2\lvert\sin 2\psi\rvert$	0	0	0
$\hat{\mathbf{w}}$	–	$\hat{\mathbf{u}}$	$2(1 + \lvert\cos 2\psi\rvert)$	0	90°	0
–	$\hat{\mathbf{w}}$	$\hat{\mathbf{u}}$	$4\lvert\sin(\cos^{-1}((1/2)\sin 2\psi))\rvert$	90°	90°	0
–	$\hat{\mathbf{u}}$	$\hat{\mathbf{w}}$	$4\lvert\sin(\cos^{-1}(\cos^2\psi))\rvert$	90°	0	0
$\hat{\mathbf{u}}$	$\hat{\mathbf{w}}$	–	$4\lvert\sin(\cos^{-1}(\sin^2\psi))\rvert$	90°	90°	90°
$\hat{\mathbf{w}}$	$\hat{\mathbf{u}}$	–	$4\lvert\sin(\cos^{-1}((1/2)\sin 2\psi))\rvert$	0	90°	90°

interpolating 'potential' of the form

$$V_{\text{int}}(\Omega) = \alpha + \beta F_1(\theta) + \gamma[F_2(\phi,\theta) + F_3(\theta,\chi)] + \delta F_4(\phi,\theta,\chi), \tag{4}$$

where [51]

$$\frac{\alpha}{2DL^2} = \frac{2}{3}\left[\lvert\sin 2\psi\rvert + 4\left|\sin\left(\cos^{-1}\left(\frac{1}{2}\sin 2\psi\right)\right)\right|\right], \tag{5}$$

$$\frac{\beta}{2DL^2} = \frac{4}{3}\left[\lvert\sin 2\psi\rvert + \left|\sin\left(\cos^{-1}\left(\frac{1}{2}\sin 2\psi\right)\right)\right|\right] - 1 - \lvert\cos 2\psi\rvert - 2\left|\sin\left(\cos^{-1}(\sin^2\psi)\right)\right|, \tag{6}$$

$$\frac{\gamma}{2DL^2} = \frac{1}{2} + \frac{1}{2}\lvert\cos 2\psi\rvert - \left|\sin\left(\cos^{-1}(\sin^2\psi)\right)\right|, \tag{7}$$

$$\frac{\delta}{2DL^2} = 1 + \lvert\cos 2\psi\rvert + 2\left|\sin\left(\cos^{-1}(\sin^2\psi)\right)\right| - 4\left|\sin\left(\cos^{-1}\left(\frac{1}{2}\sin 2\psi\right)\right)\right|, \tag{8}$$

and the angular functions $F_i(\Omega)$, which are linear combinations of the Wigner rotation functions of rank 2 [9, 47], are given by

$$F_1(\theta) = P_2(\cos\theta) = \frac{1}{2}(3\cos^2\theta - 1), \tag{9}$$

$$F_2(\phi,\theta) = \sin^2\theta\cos 2\phi, \tag{10}$$

$$F_3(\theta,\chi) = \sin^2\theta\cos 2\chi, \tag{11}$$

$$F_4(\phi,\theta,\chi)=\frac{1}{2}(1+\cos^2\theta)\cos 2\phi\cos 2\chi-\cos\theta\sin 2\phi\sin 2\chi. \tag{12}$$

This sacrifices quantitative accuracy, but preserves the correct qualitative behaviour; it is discussed in more detail in Section III.B and in the Appendix.

Note that $V_{\rm int}(\Omega)$ is in fact a *two*-particle potential; in the foregoing (as in [7]) we have just assumed that the reference particle is located at the origin of the lab-fixed frame (its general form is given by Eq. (7) of [7]). The corresponding one-particle mean-field potential. $W(\Omega)$, is then obtained by integration over the coordinates of one of the particles:

$$W(\Omega)=w_1F_1(\theta)+w_2F_2(\phi,\theta)+w_3F_3(\theta,\chi)+w_4F_4(\phi,\theta,\chi), \tag{13}$$

which yields

$$\frac{f_N[\rho,\hat{f}(\Omega)]}{k_{\rm B}T}=\frac{f_I(\rho)}{k_{\rm B}T}+\rho\langle\log[8\pi^2\hat{f}(\Omega)]\rangle+\frac{1}{2k_{\rm B}T}\rho(w_1s_1+w_2s_2+w_3s_3+w_4s_4), \tag{14}$$

where $f_1(\rho)$ is the free energy density of the isotropic phase, $\langle A(\Omega)\rangle=\int d\Omega\hat{f}(\Omega)A(\Omega)$, and the order parameters are defined as

$$s_1=\langle F_1(\theta)\rangle, \tag{15}$$

$$s_2=\langle F_2(\phi,\theta)\rangle, \tag{16}$$

$$s_3=\langle F_3(\theta,\chi)\rangle, \tag{17}$$

$$s_4=\langle F_4(\phi,\theta,\chi)\rangle, \tag{18}$$

As remarked in Refs. [7,9], s_1, the canonical nematic order parameter, and s_3, the molecular biaxiality, are associated with uniaxial order around the z-axis, whereas s_2 and s_4 signal biaxiality of the ODF around that axis: $s_1>0$ in the N_+ phase, and <0 in the N_- phase, whereas $s_2=s_4=0$ in either of these phases (see also end of Section III.A). In addition, self-consistency requires that

$$w_1=\rho(\beta s_1+\gamma s_3), \tag{19}$$

$$w_2 = \rho\left(\frac{3}{4}\beta s_2 + \gamma s_4\right), \tag{20}$$

$$w_3 = \rho\left(\gamma s_1 + \frac{3}{4}\delta s_3\right), \tag{21}$$

$$w_4 = \rho(\gamma s_1 + \delta s_3). \tag{22}$$

From functional minimisation of the free energy, Eq. (14), with respect to the ODF, we obtain

$$\hat{f}(\Omega) = \frac{\exp[-W(\Omega)/(k_B T)]}{\int d\Omega \exp[-W(\Omega)/(k_B T)]}. \tag{23}$$

The consistency equations for the order parameters, Eqs. (15–18) can now be solved, together with Eq. (23), as functions of the density ρ. This can only be done numerically, therefore in the next subsection we discuss a simpler method for locating isotropic-symmetry-breaking transitions [9].

B. Bifurcation Analysis

Bifurcation analysis provides a tool to locate phase transitions approximately, in alternative to the more computationally demanding (and sometimes not much more physically illuminating) task of solving the mean-field equations. Specifically, in the present case one looks for instabilities of the isotropic phase with respect to perturbations of (uniaxial or biaxial) nematic symmetry. The appropriate basis functions for expanding such perturbations, $\Delta^l_{\min}(\Omega)$, have been introduced by Mulder [9, 52]; for $l = 2$ they are proportional to Straley's $F_i(\Omega)$ (Eqs. (9–12)) [7]. The angle-dependent excluded volume, $v_{\text{excl}}(\Omega)$ in Eq. (3), can likewise be expressed as

$$v_{\text{excl}}(\Omega) = \sum_{l,m,n} \frac{(2l+1)}{8\pi^2} K_{l,mn} \Delta^l_{mn}(\Omega). \tag{24}$$

It is now straightforward to write the interpolating potential, Eq. (4), in terms of the functions $\Delta^2_{m,n}(\Omega)$:

$$V_{\text{int}}(\Omega) = \alpha + \beta\Delta^2_{0,0}(\Omega) + \frac{2\gamma}{\sqrt{3}}\left[\Delta^2_{0,2}(\Omega) + \Delta^2_{2,0}(\Omega)\right] + \delta\Delta^2_{2,2}(\Omega), \tag{25}$$

whence the corresponding expansion coefficients are

$$K_{0,00} = 8\pi^2\alpha, \tag{26}$$

$$K_{2,00} = \frac{8\pi^2}{5}\beta, \tag{27}$$

$$K_{2,02} = K_{2,20} = \frac{16\pi^2}{5\sqrt{3}}\gamma, \tag{28}$$

$$K_{2,22} = \frac{8\pi^2}{5}\delta. \tag{29}$$

The (reduced) bifurcation density into the $N_{\pm}$ phase then follows from Eqs. (3.9) and (3.12) in [9]:

$$c_0^* = \frac{\pi}{4}DL^2\rho_0^* = -\frac{\pi^3}{\bar{\kappa}_*}, \tag{30}$$

$$\bar{\kappa}_* = \frac{\kappa_*}{2DL^2} = \frac{1}{4DL^2}\{K_{2,00} + K_{2,22} - [(K_{2,00} - K_{2,22}) + 4K_{2,02}^2]^{1/2}\}, \tag{31}$$

and the Landau point, at which the ordering transition is continuous, from Eq. (3.23) or (3.24) in the same reference:

$$K_{2,02} = 0, \quad K_{2,00} - K_{2,22} > 0, \tag{32}$$

$$K_{2,00} - K_{2,22} = -\frac{2|K_{2,02}|}{\sqrt{3}}. \tag{33}$$

C. Numerical Calculation of the Second Virial Coefficient

The theory described in Section II.A is a simplified second virial theory. It is appropriate only for long monomers, where one can neglect the effects of overlaps of more than one pair of monomers, and it furthermore approximates the form of the angle-dependent second virial coefficient. Notwithstanding the fact that these approximations are expected not to greatly affect the general topology of the predicted phase diagram, it is of interest to

investigate how quantitatively accurate this approach might be. With this end in view, we conducted some numerical calculations of the angle-dependent second virial coefficients.

Two methods were used. In the first and crudest scheme, one imagines a cuboid surrounding a central dimer, such that a second dimer placed at any orientation outside this cuboid cannot overlap the first dimer. The second dimer is then placed in a random position within this cuboid at a random orientation and one tests for an overlap between the two dimers. This procedure is repeated a large number of times, and the ratio of overlaps to the total number of configurations is simply the ratio of the dimer–dimer excluded volume to that of the cuboid.

Although this method is good for relatively short monomers, it is not so efficient for long monomers. This is because the volume of the cuboid is proportional to the cube of the monomer length, whilst the excluded volume is proportional to the monomer length squared. Thus for long monomers, the ratio of overlapping configurations to the total number of trials is small and the whole algorithm is inefficient. To improve matters, we used the following technique. A monomer of the first dimer was placed parallel to the z-axis and a monomer of the second dimer was randomly placed subject to the conditions that the vector along its symmetry axis lay in the xz-plane and that the two monomers overlapped. This may again be achieved by positioning the second monomer at random within a cuboid centred on the first monomer, but this time the volume of the cuboid is of order DL^2. Given two overlapping monomers, one converts each monomer into a dimer by randomly attaching the cap of the partner monomer to a cap of the original monomer, but subject to the fixed bond-angle constraint. One then tests for overlap of each pair of monomers. It is a straightforward matter to decompose the total Mayer f-function $\Phi(12)$ for the two dimers in terms of Mayer f-functions and e-functions for the monomers (where $e(12) = 1 + \Phi(12)$), and this allows one to follow the methods of Ree and Hoover [53] to find the total excuded volume as a weighted sum of diagrams composed of these f and e functions. Thus while this second method is more complicated than the first, it is more efficient in the case of particles composed of long monomers. Because of this extra complexity, we were careful to check that the two algorithms gave consistent results.

As described, these methods only give the angularly averaged or isotropic excluded volume (or, equivalently, the isotropic second virial coefficient which is half the excluded volume). To obtain angular information we calculated some of the coefficients in the expansion of the angle-dependent second virial coefficients in terms of Wigner rotation functions. To do this

we chose our z-axis to be parallel to line joining the mid-points of the monomers in the first dimer and the x-axis to be along the bisector of the monomers. The y-axis was then chosen to make a right-handed coordinate system. Using the conventions of Gray and Gubbins [47], we then calculated Wigner rotation functions corresponding to the orientation of the second dimer in this coordinate system. By weighting the sums in both Monte Carlo algorithms by these functions, one can estimate the quantity B^l_{mn}, given by

$$B^l_{mn} = \frac{1}{8\pi^2} \int D^l_{mn}(\Omega) B_2(\Omega) d\Omega \tag{34}$$

where Ω represents the Euler angles of the second dimer, $B_2(\Omega)$ is the angle-dependent second virial coefficient (equal to $(1/2)v_{\text{excl}}(\Omega)$ in Eq. (3)), and D^l_{mn} is a Wigner rotation function. These coefficients are directly proportional to the expansion coefficients mentioned above.

For the simpler problem of investigating the I–N phase transition for hard spherocylinders at this level of theory, one often expands $B_2(\Omega)$ in terms of a series of spherical harmonics, but to get accurate answers one needs to include spherical harmonics up to a rank of at least 14 [54]. It is likely that contributions from Wigner rotation functions up to a similar rank would be required in order to analyse the dimer transition, at least for the case of fairly linear particles. In this paper, however, we concentrate on bond angles close to the Landau angle and in this regime the transition is mainly controlled by Wigner rotation functions of rank 2. Indeed only terms of this order were used in the preceding analytical theory.

The symmetry of the dimer implies the following restrictions on B^l_{mn}:

1. $B^l_{mn} = 0$ unless l is even;
2. B^l_{mn} is real;
3. $B^l_{mn} = B^l_{nm} = B^l_{m-n}$;
4. $B^l_{mn} = 0$ unless $m+n$ is even.

Thus for $l = 2$, the independent, non-vanishing coefficients are B^2_{22}, B^2_{20}, B^2_{11} and B^2_{00}. Unlike the more symmetric cases of an ellipsoid or a parallelepiped [9, 11], one finds here a non-vanishing B^2_{11} coefficient. This term is vanishingly small for long monomers, but non-zero for shorter ones, and originates from configurations in which more than a single pair of monomers overlap. Hence there exists the possibility that a ferroelectric phase (polar order of the short axes) might occur, but a bifurcation analysis using the numerical results obtained so far indicates that this term is always too small to allow a direct isotropic-ferroelectric transition – the normal

nematic phase always comes in first. In the following analysis we ignore the B_{11}^2 terms, as they do not contribute to the formation of either a nematic or a biaxial phase [50].

III. RESULTS

A. Analytical Treatment

All results presented in this section pertain to the Onsager limit, $L/D \to \infty$, implicit in Eq. (1). Eqs. (15–18) have been solved iteratively by increasing the reduced density c at constant $\psi \in [0, \pi/4]$, until

$$|s_i^{j+1} - s_i^j| \leq \text{Acc} \quad (i = 1 - 4), \tag{35}$$

were simultaneously satisfied, where Acc = 10^{-6} or 10^{-7} and the superscript j denotes the jth iterate. The angular integrations were performed by 16-point Gauss-Legendre quadrature [55]. In Figures 2 and 3 we show the phase diagram of HBs, in terms of the reduced density $c = (\pi/4)DL^2\rho$; as in previous work [5, 7–9, 11, 14, 15], we found N_+, N_-, and biaxial (B) phases. The solid line is the locus of the lowest densities at which Eqs. (15–18) have uniaxial nematic solutions; in this preliminary study we have not determined the binodal. The dotted lines are the loci of (continuous) uniaxial–biaxial transitions, and the dashed line is the limit of stability of the isotropic phase with respect to nematic fluctuations, from Eqs. (30) and (31) with Eqs. (27–29). Gratifyingly, all curves meet at the Landau point, predicted from bifurcation analysis (Eq. (33)) to be $\psi_{\text{Landau}} \approx 0.2018\pi = 36.32°$ ($\Psi_{\text{Landau}} \approx 107.36°$); numerically we get $\psi_{\text{Landau}} \approx 0.2016\pi$, in very good agreement. As one approaches the Landau point from either side, convergence gets very slow, requiring literally thousands of iterations to reach the desired accuracy.

A word is in order with regard to the identification of the different phases. As remarked in [9], non-vanishing s_1 and s_3 and vanishing s_2 and s_4, are associated with uniaxial order *around the z-axis*; likewise, non-vanishing s_2 and s_4 are the signature of biaxial order *around that same axis*. The system may nevertheless order uniaxially around some other axis *in which case all four order parameters would be non-zero*. They would, however, be related by the elements of the rotation matrix which transforms the basis functions $F_i(\Omega)$ between the lab-fixed frame and that in which the order parameter

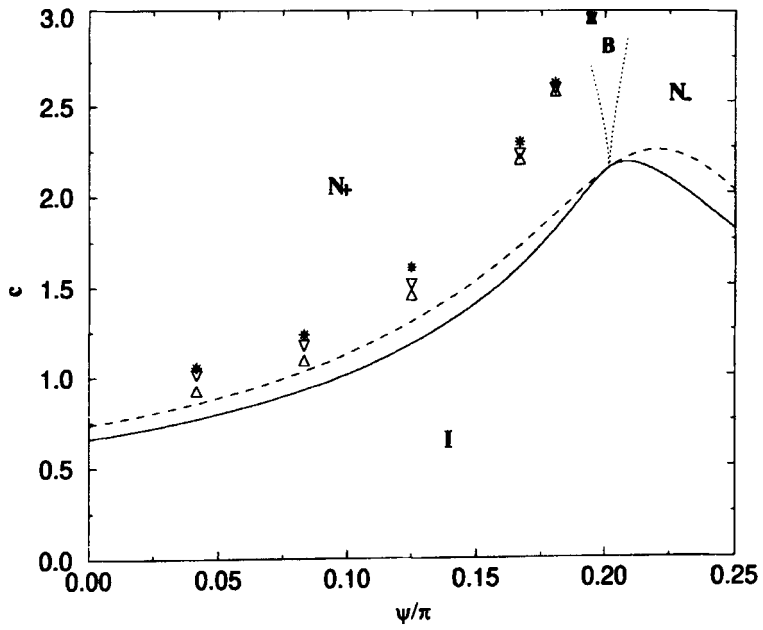

FIGURE 2 Phase diagram of the HB fluid. I: isotropic phase; N_+: rod-like uniaxial nematic phase; N_-: plate-like uniaxial nematic phase; B: biaxial nematic phase. All lines are from the analytical theory of Sections II.A and II.B, with $L/D = \infty$ (Onsager limit). Solid lines: limit of stability of the uniaxial nematic phases; dashed line: limit of stability of the isotropic phase (from bifurcation theory); dotted lines: continuous uniaxial–biaxial transitions. The symbols are numerical results pertaining to the theory of Section II.C, with Table II ($L/D = 10^6$). Stars: limit of stability of the isotropic phase from bifurcation analysis; triangles up: c_1 at $I-N_+$ coexistence; triangles down: c_N at $I-N_+$ coexistence. See the text for details.

tensor is diagonal [9]. In practice, starting the iteration with initial guesses $s_1 = s_2 = s_3 = s_4 = 0.5$ always led to a N_+ phase symmetric about the z-axis for $\psi < \psi_{\text{Landau}}$; for $\psi > \psi_{\text{Landau}}$ it led to an apparently biaxial phase (*i.e.*, all $s_i \neq 0$), but whose order parameters were related by $s_2 = 2s_1$, $s_4 = (3/2)s_3$, corresponding to N_+ order about the x-axis. This turned out to have much higher free energy than a N_- phase symmetric about the z-axis (in which s_2, $s_4 \sim 0$), resulting from the initial guesses $s_1 = s_3 = -0.5$, $s_2 = s_4 = 0.5$. Thus we have defined the $N_\pm - B$ lines, somewhat arbitrarily, as the loci of points where s_2 first exceeds 10^{-4} as the density is increased.

In Figures 4 and 5 we plot the order parameters as functions of the reduced density for two different boomerang angles ψ, on either side of the Landau point. Notice the weakening of the first-order $I-N$ transition as a consequence of particle biaxiality [16, 17].

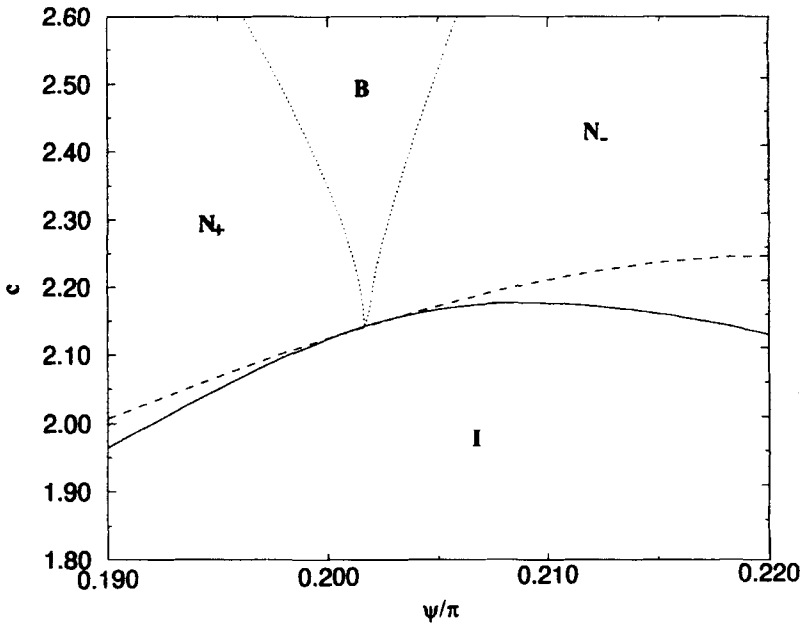

FIGURE 3 Detail of the phase diagram in the vicinity of the Landau point; same symbols as in Figure 2.

B. Numerical Calculations

To date we have numerical results for long monomers ($L/D = 10^6$) and for fairly short ones ($L/D = 2$), using the second Monte Carlo algorithm described in Section II.C. For the final averages 10^9 trial configurations were generated. Errors were estimated by splitting the total number of configurations into sub-blocks each containing 10^5 configurations and then calculating the standard error in the mean using this set of 10^4 sub-averages. Some data are presented in Tables II and III, and the coefficients are given in units of the isotropic second virial coefficient of a pair of monomers, $B_{2,\text{mon}}$, where [56]

$$B_{2,\text{mon}} = \frac{2\pi}{3}D^3 + \pi LD^2 + \frac{\pi}{4}DL^2. \tag{36}$$

The error is approximately 4×10^{-5} in all cases except B_{00}^0 for $L/D = 10^6$, for which it is 10^{-7}. Taking the long monomer data first, we see that the isotropic second virial coefficient, B_{00}^0, is equal to $4B_{2,\text{mon}}$, independent of bond angle. This follows from the fact that only overlaps of a single pair of

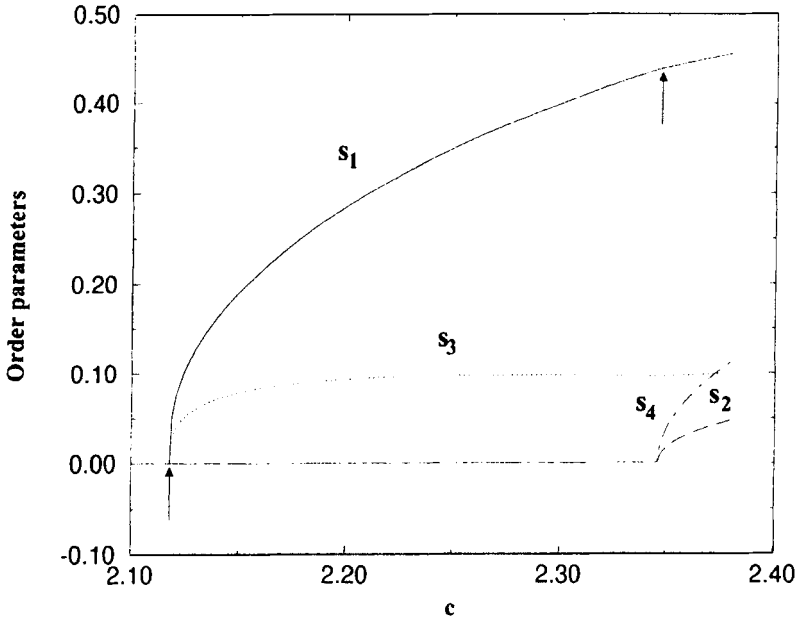

FIGURE 4 Order parameters s_1 (solid line), s_2 (dashed line), s_3 (dotted line), and s_4 (dot-dashed line) *vs.* reduced density, for $\psi = 36°$. Note the smallness of the jump at the $I-N_+$ transition, and the discontinuity in the slope of the s_1 curve at the $N_- - B$ transition (marked by arrows).

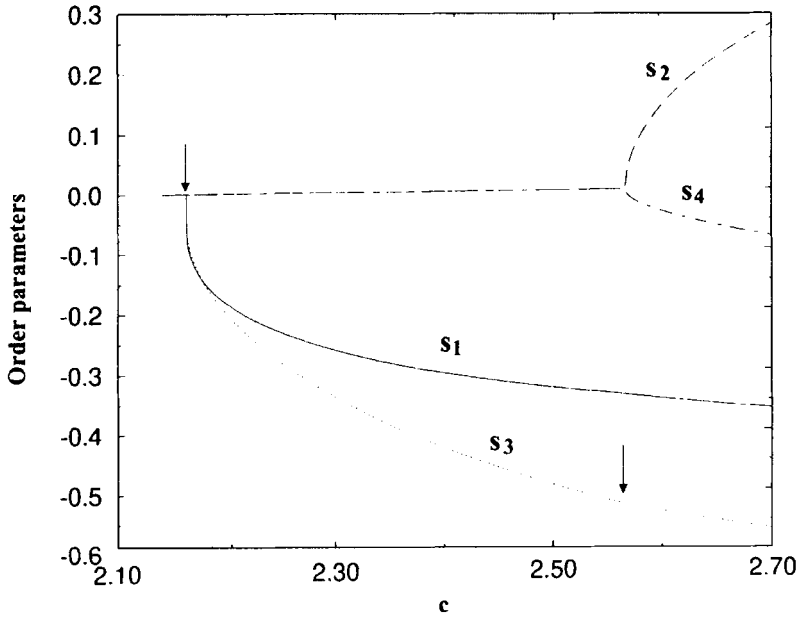

FIGURE 5 Same as in Figure 4, but for $\psi = 37°$. Besides a weak first-order $I-N_-$ transition, a 'bump' is again visible, now on the s_3 curve, at the $N_- - B$ transition (both are marked by arrows).

TABLE II Second virial data for $L/D = 10^6$: all coefficients are in units of $B_{2,\mathrm{mon}}$ (the isotropic second virial coefficient for monomers). $B^0_{00} = 4$ with an error of 10^{-7}. $c^* = B_{2,\mathrm{mon}}\rho^*$, the limit of stability of the isotropic phase with respect to (uniaxial) nematic fluctuations, and ν, are from Mulder's bifurcation analysis [9]. ν changes sign at the Landau point, whence $\Psi_{\mathrm{Landau}} \approx 100°$

$\Psi(°)$	B^2_{00}	B^2_{20}	B^2_{22}	c^*	ν
165	-0.4748	-5.05×10^{-3}	6×10^{-5}	1.053	0.999
150	-0.4046	-1.842×10^{-2}	-8.5×10^{-4}	1.231	0.981
135	-0.3045	-3.500×10^{-2}	-4.00×10^{-3}	1.600	0.885
120	-0.1953	-4.785×10^{-2}	-1.170×10^{-2}	2.286	0.540
115	-0.1607	-5.014×10^{-2}	1.558×10^{-2}	2.605	0.319
110	-0.1282	-5.100×10^{-2}	-2.029×10^{-2}	2.963	0.033
105	-9.856×10^{-2}	-5.038×10^{-2}	-2.577×10^{-2}	3.333	-0.302
90	-3.129×10^{-2}	-3.825×10^{-2}	-4.68×10^{-2}	4.003	-1

TABLE III Second virial data for $L/D = 2$: same units as in Table II (but note that now $B^0_{00} \neq 4$). c^* and ν are again given by Mulder's bifurcation analysis [9], yielding $\Psi_{\mathrm{Landau}} \approx 90°$

$\Psi(°)$	B^0_{00}	B^2_{00}	B^2_{20}	B^2_{22}	c^*	ν
165	3.2047	-0.1992	-1.71×10^{-3}	0	3.12	1
150	3.2001	-0.1788	-6.29×10^{-3}	-2.3×10^{-4}	3.487	0.99
135	3.1926	-0.1499	-1.252×10^{-2}	-1.10×10^{-3}	4.122	0.94
120	3.1789	-0.1182	-1.866×10^{-2}	-2.98×10^{-3}	5.071	0.79
105	3.1575	-8.854×10^{-2}	-2.297×10^{-2}	-6.40×10^{-3}	6.30	0.49
90	3.1252	-6.438×10^{-2}	-2.468×10^{-2}	-1.130×10^{-2}	7.62	0.024
85	3.1110	-1.323×10^{-2}	-2.463×10^{-2}	-1.323×10^{-2}	11.6	-0.88

monomers contribute to the second virial coefficient in this limit and that there are four such pairings. This result only breaks down at extremely small bond angles, when the two monomers are virtually side-by-side.

From bifurcation analysis (Section II.B and [9]), we find that the Landau angle, Ψ_{Landau}, is very close to 100° ($\psi_{\mathrm{Landau}} \approx 35°$). We also found the I–N coexistence (from Onsager theory [10]) for larger values of Ψ (Tab. IV, Figs. 2 and 6). As expected the order parameters become very small near $\Psi \sim 100°$ and the densities of the co-existing phases also have become almost identical. The analytical theory correctly captures the qualitative trend, but quantitative agreement worsens as Ψ_{Landau} is approached; furthermore, it seriously underestimates the principal nematic order parameter s_1 over most of the range of boomerang angles. (By contrast, predictions for the molecular biaxiality order parameter s_3, which remains small, are remarkably consistent). Since for $L/D = 10^6$ we are practically in the Onsager limit, where the contribution due to multiple overlaps is negligible (as can be seen from the fact that B^0_{00} is almost exactly $4B_{2,\mathrm{mon}}$), the impoverishment in performance can only be ascribed to the deteriorating quality of the interpolation formula for the excluded volume, Eq. (4), as $\Psi \to \Psi_{\mathrm{Landau}}$

TABLE IV I–N transition results for long monomers, $L/D = 10^6$: $c = B_{2,\mathrm{mon}}\rho$. Note the smallness of s_1 for $\Psi \sim \Psi_{\mathrm{Landau}} \approx 110°$

$\Psi(°)$	c_I	c_N	s_1	s_3
165	0.925	1.01	0.565	0.003
150	1.09	1.17	0.538	0.011
135	1.45	1.51	0.486	0.03
120	2.19	2.22	0.341	0.067
115	2.560	2.575	0.220	0.072
110	2.9617	2.9620	0.023	0.0142

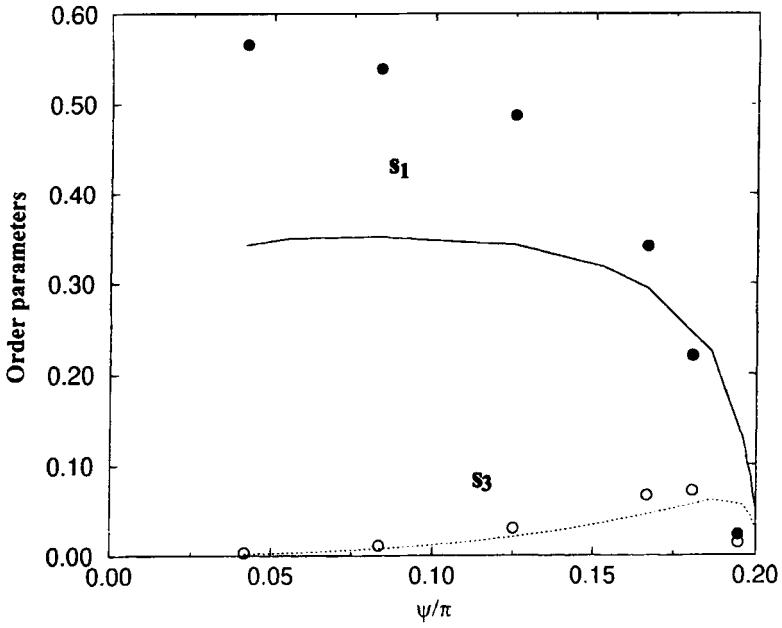

FIGURE 6 Uniaxial order parameters s_1 (solid line) and s_3 (dotted line) *vs.* ψ at limit of stability of the N_+ phase (solid line in Fig. 2), from the analytical theory of Section II.A. Symbols: s_1 (filled circles) and s_3 (open circles) at the $I-N_+$ coexistence, obtained by the numerical method of Section II.C for $L/D = 10^6$ (data from Tab. IV).

(see also the Appendix). A (plausibly) smaller source of additional error is that the results based on the interpolation formula are for a nematic phase at the lowest density for which Eqs. (15–18) have a uniaxial nematic solution. In contrast the densities given from the purely numerical approach correspond to binodal densities.

Turning next to the shorter monomer data ($L/D = 2$), we firstly notice that B_{00}^0 is no longer equal to $4B_{2,\mathrm{mon}}$, because now overlaps of more than

TABLE V I–N transition results for short monomers, $L/D = 2$: same units as in Table IV. Again, s_1 is quite small for $\Psi \sim \Psi_{\text{Landau}} \approx 90°$

$\Psi(°)$	c_I	c_N	s_1	s_3
165	2.24	2.33	0.495	0.002
150	2.50	2.58	0.486	0.010
135	2.98	3.05	0.464	0.023
120	3.734	3.797	0.415	0.044
105	4.804	4.836	0.296	0.069
90	5.93997	5.94010	0.016	0.010

one pair of monomers contribute to the overall second virial coefficient. Nevertheless it is noticeable that B_{00}^0 depends only very weakly on bond angle. Indeed recent computer simulation studies [54] indicate that the isotropic equation of state is only weakly dependent on bond angle over a wide range of packing fractions. Moreover, we find a Landau angle very close to 90°. The explicit calculation of the I–N coexistence point (Tab. V) again shows that at this angle the order parameters are very small and the densities of the co-existing phases are practically identical.

For such short dimers, however, the packing fractions at which these transitions occur are unphysically high. Indeed a second virial account is clearly inappropriate for these short particles and higher virial coefficients are needed. In future work we will investigate the effects of including the third virial coefficient and of approximately resumming the virial series, so as to compare quantitatively with computer simulation [57]. All that we wish to say at present is that the Landau angle is expected to vary with monomer length. Whether the phase diagram will look the same as that for long rods will depend on whether other phase transitions, such as crystallisation, pre-empt the liquid crystalline phase transitions considered here.

IV. CONCLUSIONS

We have developed a simple theory of the nematic ordering of HBs, which we hope can shed some light on the phase behaviour of LC dimers. As a consequence of particle biaxiality, biaxial as well as uniaxial (both rod-like and plate-like) phases have been found. Although no actual phase boundaries have been traced (apart from a small number of points), it can be concluded that the topology of the phase diagram is in agreement with that obtained in previous studies of related systems, namely hard spheroplatelets and hard biaxial ellipsoids (in the latter case both by theory

and simulation). This is in spite of several rather severe approximations introduced, namely (i) the truncation of the free energy expansion at the level of the second virial; (ii) the replacement of the excluded volume of two non-convex bodies by the sum of excluded volumes of pairs of convex constituents thereof; and (iii) the use of a low-order approximation for the latter excluded volumes. Of these, (iii) probably has the most serious (quantitative) effect, although (i) and (ii) will of course be manifest in comparisons of our theoretical predictions with molecular simulation results for finitely-long particles. We have attempted to assess the validity of (ii) and (iii) by evaluating the second virial coefficient of HBs numerically (Eq. (A9)) [58]. This revealed (iii) to become increasingly (quantitatively) unreliable as $\Psi \to \Psi_{\text{Landau}}$. Furthermore, it does *not* recover the exact relation $B_{00}^0 = 4B_{2,\text{mon}}$ except for $\Psi = 180°$. The Landau angle Ψ_{Landau} is, however, accurately located.

Acknowledgements

This work was initiated while P. I. C. Teixeira was at the FOM Institute for Atomic and Molecular Physics in Amsterdam. He thanks the Chemistry Department of Manchester University for their hospitality, and acknowledges financial support from the EPSRC. A. J. Masters is grateful to NATO for the award of a Travel Grant which made this collaboration possible. The work of the FOM Institute is part of the research programme of FOM and is supported by the Nederlandse Organisatie voor Wetenschappelijk Onderzoek (NWO). We are indebted to Ronald Blaak and Agnieszka Chrzanowska for stimulating discussions, to Geoffrey Luckhurst for providing us with Ref. [46], and to Mark Warner for a critical reading of the manuscript.

References

[1] M. J. Freiser, *Phys. Rev. Lett.*, **24**, 1041 (1970).
[2] W. Maier and A. Saupe, *Z. Naturforsch. A*, **13**, 564 (1958).
[3] W. Maier and A. Saupe, *Z. Naturorsch. A*, **14**, 882 (1959).
[4] C.-S. Shih and R. Alben, *J. Chem. Phys.*, **57**, 3055 (1972).
[5] R. Alben, *Phys. Rev. Lett.*, **30**, 778 (1973).
[6] E. F. Gramsbergen, L. Longa and W. H. de Jeu, *Phys. Rep.*, **135**, 195 (1986).
[7] J. P. Straley, *Phys. Rev. A*, **10**, 1881 (1974).
[8] N. Boccara, R. Mejdani and L. de Seze, *J. Physique*, **38**, 149 (1977).
[9] B. Mulder, *Phys. Rev. A*, **39**, 360 (1989).
[10] L. Onsager, *Ann. N. Y. Acad. Sci.*, **51**, 627 (1949).
[11] R. Holyst and A. Poniewierski, *Molec. Phys.*, **69**, 193 (1990).
[12] A. Poniewierski and R. Holyst, *Phys. Rev. Lett.*, **61**, 2461 (1988).

[13] B. M. Mulder, *Liq. Cryst.*, **8**, 527 (1990).
[14] A. Ferrarini, P. L. Nordio, E. Spolaore and G. R. Luckhurst, *J. Chem. Soc. Faraday Trans.*, **91**, 3177 (1995).
[15] F. Biscarini, C. Chiccoli, P. Pasini, F. Semeria and C. Zannoni, *Phys. Rev. Lett.*, **75**, 1803 (1995).
[16] G. R. Luckhurst, C. Zannoni, P. L. Nordio and U. Segre, *Molec. Phys.*, **30**, 1345 (1975).
[17] B. Tjipto-Margo and G. T. Evans, *J. Chem. Phys.*, **94**, 4546 (1991).
[18] J. D. Parsons, *Phys. Rev. A*, **19**, 1225 (1979).
[19] S.-D. Lee, *J. Chem. Phys.*, **87**, 4972 (1987).
[20] M. P. Allen, *Liq. Cryst.*, **8**, 499 (1990).
[21] P. J. Camp and M. P. Allen, *J. Chem. Phys.*, **106**, 6681 (1997).
[22] S.Sarman, *J. Chem. Phys.*, **104**, 342 (1996).
[23] Y. Rabin, W. E. McMullen and W. M. Gelbart, *Molec. Cryst. Liq. Cryst.*, **89**, 67 (1982).
[24] Z. Y. Chen and J. M. Deutch, *J. Chem. Phys.*, **80**, 2151 (1983).
[25] R. G. Caflish, Z. Y. Chen, A. N. Berker and J. M. Deutch, *Phys. Rev. A*, **30**, 2562 (1984).
[26] A. Stroobants and H. N. W. Lekkerkerker, *J. Phys. Chem.*, **88**, 3669 (1984).
[27] R. Hashim, G. R. Luckhurst and S. Romano, *Molec. Phys.*, **53**, 1535 (1984).
[28] P. Palffy-Muhoray, J. R. de Bruyn and D. A. Dunmur, *J. Chem. Phys.*, **82**, 5294 (1985).
[29] S. R. Sharma, P. Palffy-Muhoray, B. Bergersen and D. A. Dunmur, *Phys. Rev. A*, **32**, 3752 (1985).
[30] R. van Roij and B. Mulder, *J. Physique II*, **4**, 1763 (1994).
[31] P. J. Camp and M. P. Allen, *Physica A*, **229**, 410 (1996).
[32] P. J. Camp, M. P. Allen, P. G. Bolhuis and D. Frenkel, *J. Chem. Phys.*, **106**, 9270 (1997).
[33] A. G. Vanakaras and D. J. Photinos, *Molec. Cryst. Liq. Cryst.*, **299**, 65 (1997).
[34] P. P. Shtifanyuk and A. N. Shramkov, *Liq. Cryst.*, **12**, 477 (1992).
[35] A. Chrzanowska, *Phys. Rev. E*, in the press.
[36] L. J. Yu and A. Saupe, *Phys. Rev. Lett.*, **45**, 1000 (1980).
[37] J. Malthête, L. Liébert, A. M. Levelut and Y. Galerne, *C. R. Acad. Sci. Paris*, **303**, 1073 (1986).
[38] S. Chandrasekhar, B. K. Sadashiva, S. Ramesha and B. S. Srikanta, *Pramana, J. Phys.*, **27**, L173 (1988).
[39] S. Chandrasekhar, B. R. Ratna, B. K. Sadashiva and V. N. Raja, *Molec. Cryst. Liq. Cryst.*, **165**, 123 (1988).
[40] S. Chandrasekhar, V. N. Raja and B. K. Sadashiva, *Molec. Cryst. Liq. Cryst. Lett.*, **7**, 65 (1990).
[41] K.Praefcke, B. Kohne, B. Gündogan, D. Singer, D. Demus, S. Diele, G. Pelzl and U. Bakowsky, *Molec. Cryst. Liq. Cryst.*, **198**, 393 (1991).
[42] J.-F. Li, V. Percec, C. Rosenblatt and O. D. Lavrentovich, *Europhys. Lett.*, **25**, 199 (1994).
[43] S. M. Fan, I. D. Fletcher, B. Gündogan, N. J. Heaton, G. Kothe, G. R. Luckhurst and K. Praefcke, *Chem. Phys. Lett.*, **204**, 517 (1993).
[44] D. Demus, *Liq. Cryst.*, **5**, 75 (1990).
[45] J. W. Emsley, G. R. Luckhurst, G. N. Shilstone and I. Sage, *Molec. Cryst. Liq. Cryst.*, **102**, 223 (1984).
[46] A. Ferrarini, G. R. Luckhurst, P. L. Nordio and S. J. Roskilly, *Chem. Phys. Lett.*, **214**, 409 (1993).
[47] C. G. Gray and K. E. Gubbins, *Theory of Molecular Fluids*, Vol. 1 (Clarendon Press, Oxford, 1984).
[48] G. J. Vroege and H. N. W. Lekkerkerker, *Rep. Prog. Phys.*, **55**, 1241 (1992).
[49] R. Blaak (private communication).
[50] Note that, within our 'superposition approximation', molecules have no 'shape polarity', *i.e.*, configurations that differ by rotations of 180° about a molecular axis are indistinguishable. This is, however, not true in general (see Section II.C).
[51] We have neglected end effects.
[52] B. M. Mulder, *Liq. Cryst.*, **1**, 539 (1986).
[53] F. H. Ree and W. G. Hoover, *J. Chem. Phys.*, **49**, 639 (1964).

[54] H. N. W. Lekkerkerker, Ph. Coulon and R. van der Haegen, *J. Chem. Phys.*, **80**, 3427 (1984).
[55] W. H. Press, S. A. Teukolsky, W. T. Vetterling and B. P. Flannery, *Numerical Recipes: The Art of Scientific Computing*, 2nd edition (Cambridge University Press, 1992).
[56] In the limit of large elongations, $L/D \to \infty$, $B_{2,\mathrm{mon}}$ reduces to $(\pi/4)DL^2$, the unit of density of the preceding subsection.
[57] M. P. Allen, P. J. Camp and A. J. Masters (unpublished).
[58] An alternative route would involve examination of higher-order terms in the corresponding diagrammatic expansion [49].
[59] This is basically equivalent to comparing the exact and approximate B_{00}^0 (see Eq. (34)).

APPENDIX: ACCURACY OF THE INTERPOLATION OF THE EXCLUDED-VOLUME INTERACTION

Let i_j denote the jth segment of particle i, and start by placing particle 1 at the origin of the lab frame. Then its constituent segments are given by (see Fig. 1)

$$\Omega_{1_1} = (\phi_1 = 0, \theta_1 = \psi, \chi_1 = 0) = (x_1 = L\sin\psi, y_1 = 0, z_1 = L\cos\psi), \quad \text{(A1)}$$

$$\Omega_{1_2} = (\phi_2 = 0, \theta_2 = \pi - \psi, \chi_2 = 0) = (x_2 = L\sin\psi, y_2 = 0, z_2 = -L\cos\psi). \quad \text{(A2)}$$

Now we want to find the Euler angles pertaining to the constituent segments of particle 2, knowing that particle 2 is connected to some frame rotated by $\Omega = (\phi, \theta, \chi)$ relative to the lab frame. Particle 2 has exactly the same coordinates as particle 1, but in the rotated frame; to find the angles between the constituent segments of the two particles, and therefrom the corresponding excluded volumes, we need to express all coordinates in the same frame. The coordinates in different frames are related by Eq. (A.123) in [47] (NB: in this reference the convention of *passive* rotations is adhered to). So we unrotate the frame connected with particle 2 to bring it into coincidence with that of particle 1. This yields

$$L^{-1}\Omega_{2_1} = \begin{pmatrix} (\cos\phi\cos\theta\cos\chi - \sin\phi\sin\chi)\sin\psi + \cos\phi\sin\theta\cos\psi \\ (\sin\phi\cos\theta\cos\chi + \cos\phi\sin\chi)\sin\psi + \sin\phi\sin\theta\cos\psi \\ -\sin\theta\cos\chi\sin\psi - \cos\theta\cos\psi \end{pmatrix}, \quad \text{(A3)}$$

$$L^{-1}\Omega_{2_2} = \begin{pmatrix} (\cos\phi\,\cos\theta\cos\chi - \sin\phi\sin\chi)\sin\psi - \cos\phi\sin\theta\cos\psi \\ (\sin\phi\,\cos\theta\,\cos\chi + \cos\phi\,\sin\chi)\sin\psi - \sin\phi\,\sin\theta\cos\psi \\ -\sin\theta\,\cos\chi\,\sin\psi - \cos\theta\,\cos\psi \end{pmatrix}. \tag{A4}$$

It follows that the angles $\Gamma_{1_i 2_j}$ between segments are

$$\begin{aligned} \cos\Gamma_{1_1 2_1} = L^{-2}\Omega_{1_1}\cdot\Omega_{2_1} &= (\cos\phi\,\cos\theta\,\cos\chi - \sin\phi\,\sin\chi)\sin^2\psi \\ &+ \cos\phi\,\sin\theta\,\sin\psi\,\cos\psi - \sin\theta\,\cos\chi\,\sin\psi\,\cos\psi \\ &+ \cos\theta\,\cos^2\psi, \end{aligned} \tag{A5}$$

$$\begin{aligned} \cos\Gamma_{1_1 2_2} = L^{-2}\Omega_{1_2}\cdot\Omega_{2_2} &= (\cos\phi\,\cos\theta\,\cos\chi - \sin\phi\,\sin\chi)\sin^2\psi \\ &- \cos\phi\,\sin\theta\,\sin\psi\,\cos\psi - \sin\theta\,\cos\chi\,\sin\psi\cos\psi \\ &- \cos\theta\,\cos^2\psi, \end{aligned} \tag{A6}$$

$$\begin{aligned} \cos\Gamma_{1_2 2_1} = L^{-2}\Omega_{1_2}\cdot\Omega_{2_1} &= (\cos\phi\,\cos\theta\,\cos\chi - \sin\phi\,\sin\chi)\sin^2\psi \\ &+ \cos\phi\,\sin\theta\,\sin\psi\,\cos\psi + \sin\theta\,\cos\chi\,\sin\psi\cos\psi \\ &- \cos\theta\,\cos^2\psi, \end{aligned} \tag{A7}$$

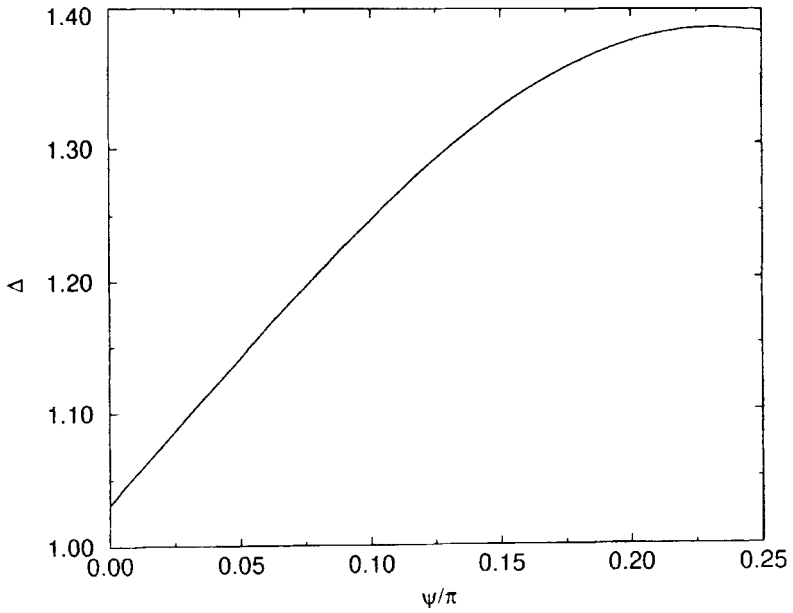

FIGURE 7 'Standard deviation' Δ *vs.* boomerang angle ψ.

$$\begin{aligned}\cos\Gamma_{1_2 2_2} = L^{-2}\Omega_{1_2}\cdot\Omega_{2_2} = (\cos\phi\cos\theta\cos\chi - \sin\phi\sin\chi)\sin^2\psi \\ - \cos\phi\sin\theta\sin\psi\cos\psi + \sin\theta\cos\chi\sin\psi\cos\psi \\ + \cos\theta\cos^2\psi.\end{aligned} \tag{A8}$$

In our 'superposition approximation', the excluded volume of two HBs is just the sum of the excluded volumes of pairs of spherocylinders, whence

$$\frac{V_{\text{excl}}(\Omega)}{2DL^2} = |\sin\Gamma_{1_1 2_1}| + |\sin\Gamma_{1_1 2_2}| + |\sin\Gamma_{1_2 2_1}| + |\sin\Gamma_{1_2 2_2}|. \tag{A9}$$

To effect the comparison between $V_{\text{excl}}(\Omega)$ and Eq. (4), we evaluate [59]

$$\Delta^2 = 2\frac{\int d\Omega\{[V_{\text{int}}(\Omega)]^2 - [V_{\text{excl}}(\Omega)]^2\}}{\int d\Omega\{[V_{\text{int}}(\Omega)]^2 + [V_{\text{excl}}(\Omega)]^2\}}. \tag{A10}$$

In Figure 7 we plot $\Delta(=\sqrt{\Delta^2})$ *vs.* ψ: the fit worsens ψ increases, consistently with Figure 2 and Table IV.